Molecular Basis for Allosteric Inhibition of GTP-Bound H-Ras Protein by a Small-Molecule Compound Carrying a Naphthalene Ring

Matsumoto, Shigeyuki ; Hiraga, Toshiki ; Hayashi, Yuki ; Yoshikawa, Yoko ; Tsuda, Chiemi ; Araki, Mitsugu ; Neya, Masahiro ; Shima, Fumi ;…

(Citation)
Biochemistry,57(36):5350-5358

(Issue Date)
2018-09-11

(Resource Type)
journal article

(Version)
Accepted Manuscript

Molecular Basis for Allosteric Inhibition of GTP-Bound H-Ras Protein by a Small-Molecule Compound Carrying a Naphthalene Ring

Shigeyuki Matsumoto[1, 3], Toshiki Hiraga[1], Yuki Hayashi[1], Yoko Yoshikawa[1], Chiemi Tsuda[1], Mitsugu Araki[2, 4], Masahiro Neya[2], Fumi Shima[1, 5], and Tohru Kataoka[1, 6, 7]

From the [1]Division of Molecular Biology, Department of Biochemistry and Molecular Biology, Kobe University Graduate School of Medicine, 7-5-1 Kusunoki-cho, Chuo-ku, Kobe 650-0017, Japan and the [2]Medicinal Frontier Dept., KNC Laboratories Co., Ltd., 1-1-1 Murotani, Nishi-ku, Kobe 651-2241, Japan

Running title: Inhibition of Ras by a naphthalene-containing compound

[3]Present address: RIKEN Cluster for Science, Technology and Innovation Hub, 53 Shogoin-Kawaharacho, Sakyo-ku, Kyoto 606-8507, JAPAN

[4]Present address: Graduate School of Medicine, Kyoto University, 53 Shogoin-Kawaharacho, Sakyo-ku, Kyoto 606-8507, JAPAN

[5]Present address: Drug Discovery Science, Division of Advanced Medical Science, Department of Science, Technology and Innovation, Graduate School of Science, Technology and Innovation, Kobe University, 7-5-1 Kusunoki-cho, Chuo-ku, Kobe 650-0017, Japan

[6]Present address: Kobe University Incubation Center, 1-5-6 Miyakojima Minami-cho, Chuo-ku, Kobe 650-0047, Japan

[7]To whom correspondence should be addressed: Prof. Tohru Kataoka, Division of Molecular Biology, Department of Biochemistry and Molecular Biology, Kobe University Graduate School of Medicine, 7-5-1 Kusunoki-cho, Chuo-ku, Kobe 650-0017, Japan, Telephone: +81-78-382-5380; Fax : +81-78-382-5399; E-mail: kataoka@people.kobe-u.ac.jp

Keywords: Ras, small GTPases, NMR, solution structure, inhibitor, naphthalene ring

ABSTRACT

The *ras* oncogene products (H-Ras, K-Ras and N-Ras) have been regarded as some of the most promising targets for anticancer drug discovery because their activating mutations are frequently found in human cancers. Nonetheless, molecular targeted therapy for them is currently unavailable. Here, we report the discovery of a small-molecule compound carrying a naphthalene ring, named KBFM123, which binds to the GTP-bound form of H-Ras. The solution structure of its complex with the guanosine 5'-(β, γ-imide) triphosphate-bound form of H-RasT35S (H-RasT35S•GppNHp) indicates that the naphthalene ring of KBFM123 interacts directly with a hydrophobic pocket located between Switch I and Switch II and allosterically inhibits the effector interaction by inducing conformational changes in Switch I and its flanking region in the β2-strand, which are directly

involved in recognition of the effector molecules including c-Raf-1. In particular, Asp38 of H-Ras, a crucial residue for the interaction with c-Raf-1 by forming a salt bridge with Arg89 of the Ras-binding domain (RBD) of c-Raf-1, shows a drastic conformational change: its side chain orients toward the opposite direction. Consistent with these results, KBFM123 exhibits an activity to inhibit, albeit weakly, the association of H-RasG12V•GppNHp with c-Raf-1 RBD. The binding of the naphthalene ring to the hydrophobic pocket of H-RasT35S•GppNHp is further supported by NMR analyses showing that two other naphthalene-containing compounds with distinct structures also exhibit similar binding properties with KBFM123. These results indicate that the naphthalene ring could become a promising scaffold for the development of Ras inhibitors.

For Table of Contents use only

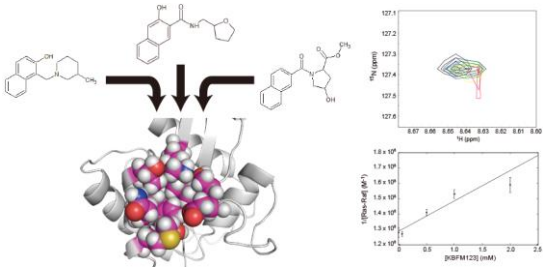

INTRODUCTION

The Ras small GTPases (H-Ras, K-Ras and N-Ras) are the products of the *ras* proto-oncogenes and function as guanine nucleotide-dependent molecular switches for regulation of cell proliferation and survival by interconverting between GTP-bound active and GDP-bound inactive forms (Ras•GTP and Ras•GDP, respectively) [1]. Ras•GTP interacts directly with effector molecules including Raf kinases (c-Raf-1, B-Raf and A-Raf), PI3Ks[1], RalGDSs and phospholipase Cε, thereby activating diverse downstream signaling pathways. The GDP-GTP cycle of Ras is reciprocally controlled by GEFs and GAPs. GEFs stimulate GDP dissociation to generate nucleotide-free Ras and thereby accelerate incorporation of GTP, which exists much more abundantly than GDP in cells. Conversely, GAPs facilitate inactivation of Ras by accelerating its intrinsic GTP-hydrolyzing activity. Oncogenic mutations, such as G12V and Q61L, drastically impair the GAP-assisted GTP hydrolysis, causing the constitutive activation of Ras [1]. Since such activating mutations are found in about 20% of human cancers, Ras has been regarded as one of the most promising target for anticancer drug development, however, no effective therapy targeting it is available at present. The interaction of Ras•GTP with the effectors is mainly mediated by two flexible regions called Switch I (residues 32-38) and Switch II (residues 60-75), which exhibit marked structural differences between Ras•GTP and Ras•GDP [2-5].

^{31}P NMR studies showed that Ras in complex with GTP or its non-hydrolyzable analogue GppNHp exhibits dynamic equilibrium between at least two distinct conformational states, called state 1 and state 2 [6, 7]. Because the association of Ras•GTP with the RBD of c-Raf-1 or RalGDS shifted the equilibrium toward state 2, it was thought that state 2 represents an active conformation capable of

interacting with the effectors while state 1 represents an inactive conformation [6, 8]. State 1 seems to form a stable pool of Ras•GTP in the GDP/GTP cycle [9]. Comparison of the crystal structures between state 1 and state 2 revealed that the most fundamental feature distinguishing state 1 from state 2 is the loss of the direct and Mg^{2+}-coordinated indirect hydrogen-bonding interactions of Thr35 in Switch I with the γ-phosphate of GTP or GppNHp [5, 10-13]. Disruption of the Thr35-γ-phosphate interaction by means of substitution mutations such as T35S induced a marked shift of the conformational equilibrium toward state 1 [5, 10-13]. In the state 1 structure, the loss of the Thr35-γ-phosphate interaction resulted in marked deviation of the Switch I loop away from the guanine nucleotide and formation of a surface pocket amenable to drug targeting, which is unseen in the state 2 structure [9, 14, 15]. This prompted us to develop allosteric Ras inhibitors targeting the state 1-specific pocket based on a working hypothesis that they would hold Ras in the state 1 conformation and interfere with the formation of state 2, thereby inactivating Ras. As a result, we successfully developed Kobe-family compounds, represented by Kobe0065 and Kobe2602, which directly bound to H-Ras•GppNHp and inhibited the binding of the effectors including Raf, PI3K and RalGDS by an *in silico* screen targeting the state 1-specific pocket [16]. Moreover, these compounds exhibited an antitumor activity toward a xenograft of a human colon cancer cell line carrying the K-*ras*G12V gene. During the course of the screening, we found a series of small-molecule compounds carrying a naphthalene ring, whose structures were distinct from those of Kobe-family compounds, exhibiting a binding activity to H-Ras•GppNHp by NMR analyses.

In the present study, we analyze the molecular mechanism for the action toward H-Ras of one of these compounds, named KBFM123, which is capable of inhibiting, albeit weakly, the binding of H-RasG12V•GppNHp to c-Raf-1 RBD. The structural information obtained will be useful for the rational development of novel Ras inhibitors by fragment-based drug design, such as fragment linking, merging and growing.

EXPERIMENTAL PROCEDURES

Preparation of Ras Proteins----Truncated forms of H-RasWT and H-RasT35S corresponding to residues 1-166 were used for the structural studies, while full-length H-RasG12V was used for the Ras-Raf binding inhibition assays. These proteins were expressed in *Escherichia coli* BL21 (DE3) as GST-fusions by using pGEX-6P-1 vector (GE Healthcare, Buckinghamshire, UK). For uniform labeling of the proteins by ^{15}N or $^{13}C/^{15}N$, *E. coli* cells were cultured in M9 minimal media containing [^{13}C]glucose (3.0 g/L) and/or [^{15}N]NH_4Cl (1.0 g/L) as the sole carbon and nitrogen sources, respectively. Supernatants after centrifugation of the sonicated cells were incubated with glutathione-Sepharose 4B resin (GE Healthcare), and the bound proteins were eluted by on-column cleavage with Turbo3C protease (Accelagen, California, USA). Further purification was achieved by chromatography on a HiTrap Q HP column (GE Healthcare). The purified H-Ras proteins were loaded with GppNHp as described [23].

NMR Spectroscopy----NMR samples were prepared in the NMR measurement buffer [25 mM

phosphate buffer, pH 6.8, 50 mM NaCl and 10 mM $MgCl_2$] in the presence of 10% D_2O and 10% d_6-DMSO. The NMR measurements were carried out on a Bruker AVANCE III 600 instrument equipped with shielded gradient triple-resonance probes. The ^{1}H signal assignments of KBFM123 were achieved by using a series of spectra, double quantum filtered COSY, ^{1}H-^{13}C HSQC, HMBC and NOESY, acquired in the NMR measurement buffer in the presence of 80% D_2O and 20% d_6-DMSO. Initial ^{1}H-^{15}N HSQC-based screening of fragment compounds was carried out at 25°C on 40 μM H-RasT35S•GppNHp mixed with the compounds at the apparent concentrations of 4 mM. The subsequent titration experiments were carried out at 25°C on 40 μM H-RasT35S•GppNHp mixed with 0.5 mM to 1.7 mM KBFM123. The CSPs were calculated as $\Delta\delta_{NH} = \sqrt{(\Delta\delta_H)^2 + (\Delta\delta_N/5)^2}$, where $\Delta\delta_H$ and $\Delta\delta_N$ are the changes in the chemical shift values for ^{1}H and ^{15}N, respectively. Significant changes in CSPs were defined as the values higher than the sum of the average and the standard deviation. The H-RasT35S•GppNHp specimens for obtaining the intermolecular NOEs with ^{13}C-edited NOESY-HSQC and 2D homonuclear NOESY spectra (mixing time 250 msec) at 5°C were prepared as described previously [16]. ^{1}H STD experiments were carried out at 5°C on 400 μM KBFM123 mixed with 20 μM H-RasT35S•GppNHp in the presence of 90% D_2O and 10% d_6-DMSO. Saturation of protein resonances was achieved by selective irradiation at the frequency of 0 ppm (on resonance) for 3 s with a 30 ms Gaussian-shaped pulse. A 10 ms spin-lock pulse was used for the suppression of the protein signals. The STD spectrum was shown by subtracting the on-resonance spectrum from the off-resonance spectrum, which is acquired by selective irradiation at the frequency of -30 ppm. The NMR spectra were analyzed with NMRPipe [24] and NMRView (One Moon Scientific, Inc., New Jersey, USA).

Structure Calculation----The intraprotein distance restraints and backbone torsion angle restraints, which were derived from the spectra in the absence of DMSO at 25°C [14, 16], were incorporated into the initial structure calculation and further optimized in the process of the subsequent calculations. The NOEs were converted into distance restraints of 1.8-2.8, 1.8-3.4 and 1.8-5.0 Å according to the signal intensities. Structural calculations were carried out by the program CNS 1.2 [25]. The CNS topology and parameter files for KBFM123 and GppNHp were generated by using Molecular Operating Environment (MOE) software package (Chemical Computing Group Inc., Montreal, Canada) and HIC-Up server [26]. The 15 structures with the lowest target function (http://www.rcsb.org, PDB code: 5ZC6) were validated by PROCHECK-NMR [27]. The structural analyses were carried out by using MOLMOL [28] and PyMOL (DeLano Scientific, LLC).

ELISA---Protein specimens for ELISA were prepared in 50 mM Tris-HCl, pH 7.4, 150 mM NaCl, 5 mM $MgCl_2$, 1 mM EDTA, 0.01% Triton X-100 and 10% DMSO. GppNHp-loaded full-length H-RasG12V (17.5 ng/well) was mixed with KBFM123 at the final concentrations ranging from 0.0625 mM to 2.0 mM. After 0.5 h of incubation at 30°C, the solution was added to a 96-well glutathione-coated plate (ThermoFisher Scientific, Waltham, MA, USA) on which GST-c-Raf-1-RBD (15 μg/well) had been immobilized. After washing to remove unbound H-Ras, the plate was incubated with a rabbit anti-H-Ras C20 antibody (#SC-520, Santa Cruz Biotech., CA, USA), raised against the

C-terminus of H-Ras, followed by a horse radish peroxidase-conjugated donkey anti-rabbit IgG antibody (GE Healthcare). The amounts of bound H-Ras were quantified by measurement of the absorbance at 450 nm with a POLARstar Omega plate reader (BMG labtech, Offenburg, Germany) after color development using the ELISA POD Substrate TMB Kit (HYPER) (Nacalai Tesque, Kyoto, Japan). Analysis of the binding kinetics was carried out as described [16].

RESULTS

Binding of KBFM123 to H-Ras•GppNHp via the Naphthalene Ring ----We found KBFM123 exhibiting a binding activity toward H-RasT35S•GppNHp by NMR-based screening of our in-house fragment library (Fig. 1*A*). The addition of 4 mM KBFM123 induced significant CSPs on the ^{1}H-^{15}N HSQC spectrum of H-RasT35S•GppNHp (Fig. 1*B*). Residues exhibiting the CSPs were mapped onto the solution structure of H-RasT35S•GppNHp based on the previous signal assignments [14], and the result indicated that KBFM123 interacted with the central β-sheet, containing Lys5, Val7, Ser39, Tyr40, Ile55, Asp57 and Thr58, and its nearby region in the C terminus of the α2-helix in Switch II, containing Thr74 and Gly75 (Fig. 1*C, D*). The CSPs were also observed for the residues spatially adjacent to these regions, including Glu62, Glu63, Tyr64, Arg68, Val103 and Lys104 (Fig. 1*C, D*). Moreover, the binding of KBFM123 was observed on the ^{1}H-^{15}N HSQC spectrum of H-RasWT•GppNHp although some of the corresponding signals were either broadened or overlapped, and the directions and extents of the CSPs were almost identical to those observed with H-RasT35S•GppNHp (Fig. S1), indicating that KBFM123 bound to H-RasWT•GppNHp with a nearly identical binding mode. Since the structure of the estimated binding regions was not considerably affected by the state transition [9] (Fig. S2), KBFM123 was likely to bind to Ras in a state-independent manner. Accordingly, we decided to utilize H-RasT35S•GppNHp instead of H-RasWT•GppNHp in further NMR experiments to avoid experimental difficulties arising from splitting or broadening of the signals from Switch regions caused by the state transition, which occurs on a millisecond time scale. A titration experiment with KBFM123 on H-RasT35S•GppNHp demonstrated progressive changes in the signal positions (Fig. 2). However, the experimental data failed to follow the first order reaction kinetics with respect to the KBFM123 concentration. Moreover, the signal of Asp57 showed nonlinear changes in the titration experiments (Fig. 2*B*), suggesting the existence of two or more processes such as conformational changes during the binding reaction. The binding of KBFM123 to H-RasT35S•GppNHp was also observed in a ^{1}H STD experiment (Fig. 3). Based on the ^{1}H signal assignments of KBFM123 (Fig. S3), signals arising from the protons on the naphthalene ring were observed in the STD spectrum while those from the rest of the chemical structure exhibited only faint signals, indicating that the naphthalene moiety was positioned at the binding interface in the complex and responsible for the interaction with H-RasT35S•GppNHp. This was strongly supported by an experiment showing that other naphthalene analogues carrying distinct substituents, KBFM59 and KBFM198, also caused CSPs similar to those of KBFM123 in the ^{1}H-^{15}N HSQC spectrum of H-RasT35S•GppNHp (Figs. 1*C* and S4). Also, the directions and degrees of the

signal changes were nearly identical to those induced by KBFM123-binding (Figs. S4 and S5), indicating that the naphthalene moieties of these compounds exhibited a similar binding mode.

Figure 1

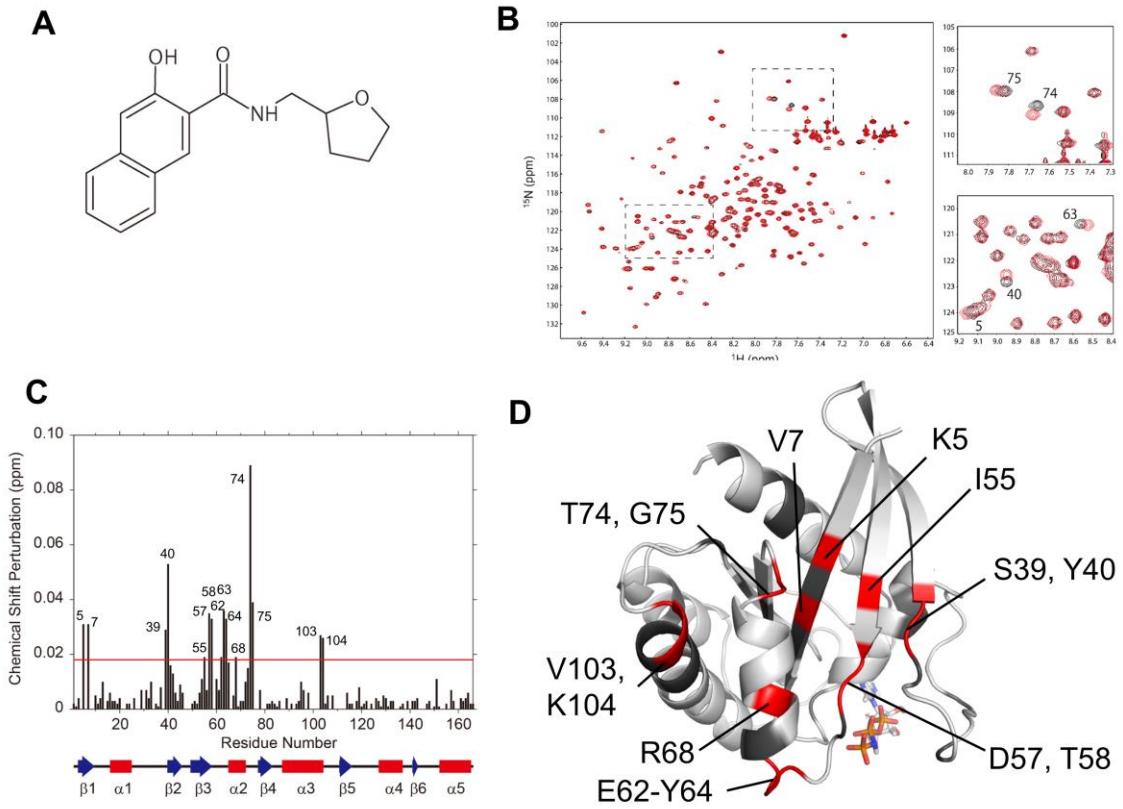

FIGURE 1. Mapping of the KBFM123-binding site on H-RasT35S•GppNHp. *A,* The chemical structure of KBFM123. *B*, Superimposition of the ^{1}H-^{15}N HSQC spectra of H-RasT35S•GppNHp in the presence (*red*) or absence (*black*) of 4 mM KBFM123. The right panels show magnifications of the regions indicated by the dashed rectangles and the signals showing significant CSPs are labeled by residue numbers. *C*, The CSPs of the NH signals induced by the binding of KBFM123. The red horizontal line indicates the sum of the average and the standard deviation. A diagram representing the secondary structure of H-RasT35S•GppNHp (PDB code 2LCF) is shown at the bottom, where α-helices and β-strands are indicated by red rectangles and blue arrows, respectively. *D*, Mapping of the CSPs onto the tertiary structure of H-RasT35S•GppNHp. Residues exhibiting significant NH signal changes are colored in red, while residues excluded from the analysis because of the signal overlapping or broadening are colored in black. GppNHp is shown in a stick model where nitrogen and oxygen atoms are colored by blue and red, respectively.

Figure 2

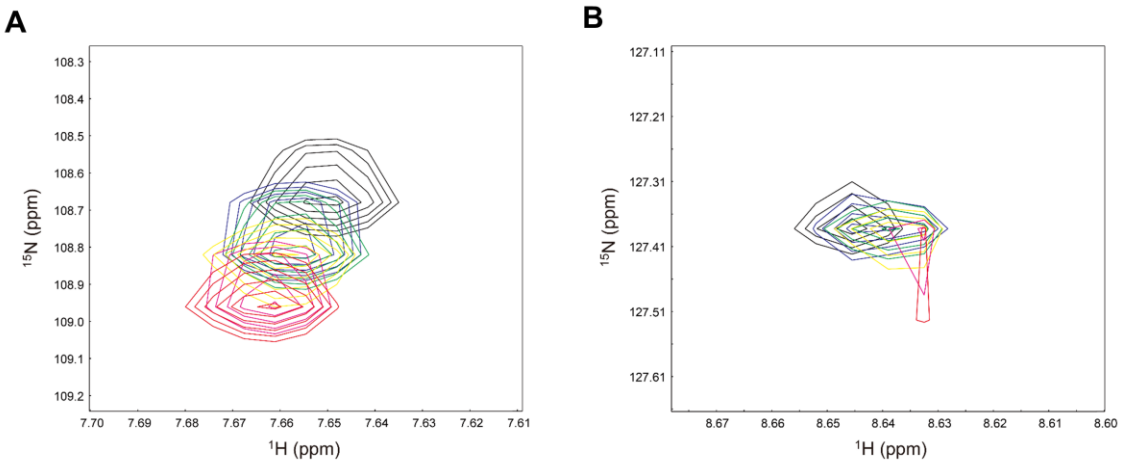

FIGURE 2. Dose-dependent signal changes of Thr74 and Asp57. The signals of Thr74 (*A*) and Asp57 (*B*) at the KBFM123 concentrations of 0 mM (*black*), 0.5 mM (*blue*), 0.7 mM (*green*), 1.0 mM (*yellow*), 1.5 mM (*magenta*) and 1.7 mM (*red*) are overlaid.

Figure 3

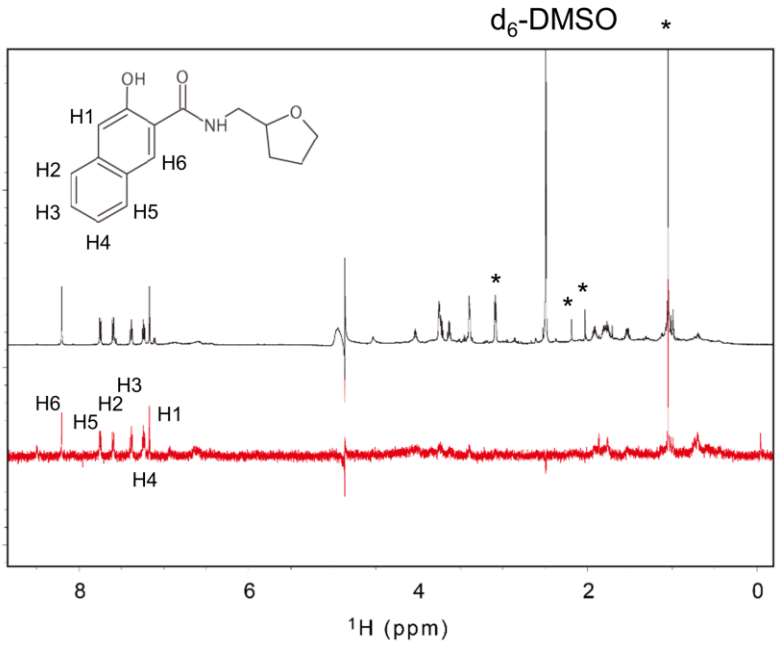

FIGURE 3. Identification of the binding epitope in KBFM123 by the STD experiment. One-dimensional proton and STD spectra are indicated in black and red colors, respectively. The proton signals observed in the STD spectrum are labeled according to the assignments shown in Fig. S3. The impurities are indicated by asterisks (*).

The Solution Structure of GppNHp-Bound H-RasT35S Complexed with KBFM123----To obtain further information on the binding mode, we determined the solution structure of the KBFM123-H-RasT35S•GppNHp complex by using NMR. One hundred twenty-four pairs of torsion angle restraints and 2591 distance restraints derived from NOE crosspeaks, including 15 intermolecular NOEs between the protons of the naphthalene ring and of H-RasT35S•GppNHp, were used for the structure calculations (Tables 1 and S1). In the final 15 structures with the lowest energies of target function, a region composed of Met1-Val9, Gly15-Asp30, Ser39-Ala59, Glu76-Asp105, Asp108-Asp119 and Arg123-His166 showed good convergence with a root-mean-square-deviation value of 0.47 ± 0.08 Å for the backbone atoms while two Switch regions and regions corresponding to Gly10-Val14, Ser106-Asp107 and Leu120-Ala122 showed poor convergence (Fig. 4*A*). Although the overall structure was similar to the previously reported solution structure of H-RasT35S•GppNHp alone (PDB code 2LCF), the N-terminal half of the β2 strand, Tyr40-Lys42, flanking Switch I was unstructured in the present structure based on the secondary structure assignments with the DSSP algorithm [17] (Fig. 4*B*). Analysis of the dihedral angle order parameter [18] showed that Switch I and its neighboring regions were rather well-defined in the present structure while the corresponding regions adopted highly divergent conformations in the solution structure of H-RasT35S•GppNHp alone [14] (Fig. 4*C*).

The structure of the KBFM123-H-RasT35S•GppNHp complex demonstrated that KBFM123 bound to H-RasT35S•GppNHp via the naphthalene ring (Fig. 5*A, B*), which was consistent with the observation with the ^{1}H STD and ^{1}H-^{15}N HSQC experiments (Figs. 1, 3, S4 and S5). On the other hand, the substituents of the naphthalene ring were oriented toward the bulk solvent and appeared to be not significantly involved in the interaction, which also agreed well with the results of the ^{1}H STD experiment (Figs. 3 and 5*A, B*). Hydrophobic interaction between the naphthalene ring and the hydrophobic cluster, mainly composed of the side-chains of Leu56 on the central β sheet and Met67, Tyr71 and Thr74 in Switch II, seemed to provide the major binding force (Fig. 5*A, B*). Structural comparison between H-RasT35S•GppNHp in the presence and absence of KBFM123 suggested that the hydrophobic cluster might be formed in response to the KBFM123-binding as follows: the orientation of the methyl group of Met67 and Thr74 shifted toward Leu56 and the aromatic side-chain of Tyr71 shifted its position to avoid the steric hindrance with Met67 and Thr74 (Fig. 5*C*). In addition, the hydrophobic portions of the side-chains of Lys5 and Ser39 in the central β sheet, Asp38, and Gln70 in Switch II also contributed to the formation of the hydrophobic cluster (Fig. 5*A, B*). Inspection of the individual structures in the ensemble showed that the side-chains of Asp38 were oriented toward Switch II and had a potential to interact with the side-chains of Tyr71 while those of Asp38 in the absence of KBFM123 were oriented toward the opposite direction and failed to make any interactions (Figs. 5*D* and S6). These inter- and intra-molecular interactions formed by Asp38 in the KBFM123 complex, albeit of rather transient nature, are expected to stabilize Switch I, which is likely to account for the convergence of the dihedral angles in the ensemble structure of Switch I and its neighboring regions to some extent (Fig. 4*C*).

Figure 4

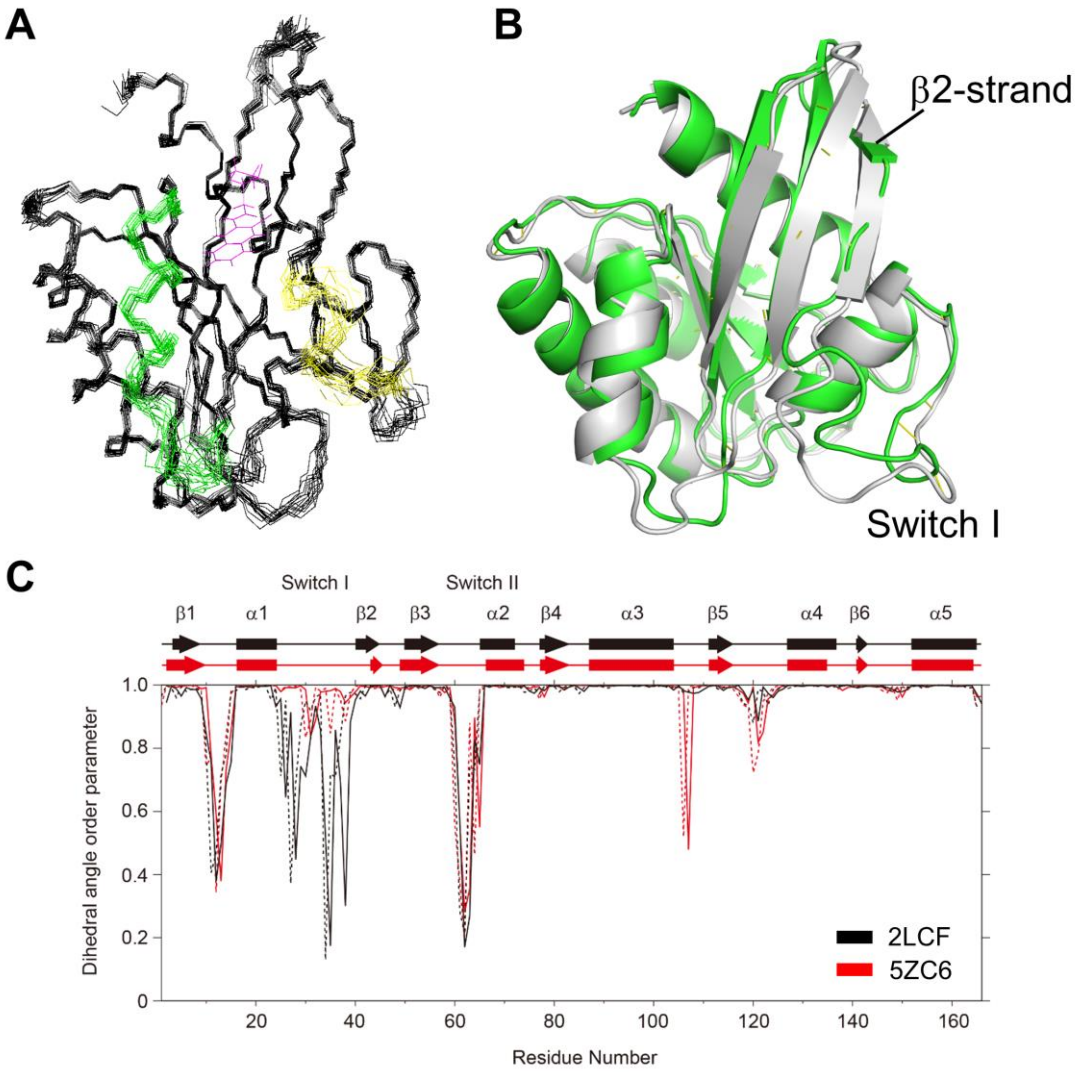

FIGURE 4. The solution structure of H-RasT35•GppNHp in complex with KBFM123. *A*, The ensemble of 15 structures with the lowest energy of the target function. A representative model of KBFM123 is shown by a magenta color. Switch I, Switch II and KBFM123 are colored in yellow, green and magenta, respectively. *B*, Superimposition of the overall structure of H-RasT35•GppNHp in the absence (PDB code 2LCF, *grey*) or presence (*green*) of KBFM123. The secondary structures were assigned with the DSSP algorithm [28] and schematically depicted at the top of the plot in *C*. *C*, Dihedral angle order parameters for the ensemble structures of H-RasT35•GppNHp in the presence (*red*) or absence (*black*) of KBFM123. The order parameters adopted values ranged from 0 to 1 and the value 1 indicates that the dihedral angles in the ensemble structure are identical. φ and ψ dihedral angles are indicated by solid and dashed lines, respectively. Diagrams representing their secondary structures are shown at the top, where the colors are identical to those of the lines in the plot, and α-helices and β-strands are indicated by rectangles and arrows, respectively.

Figure 5

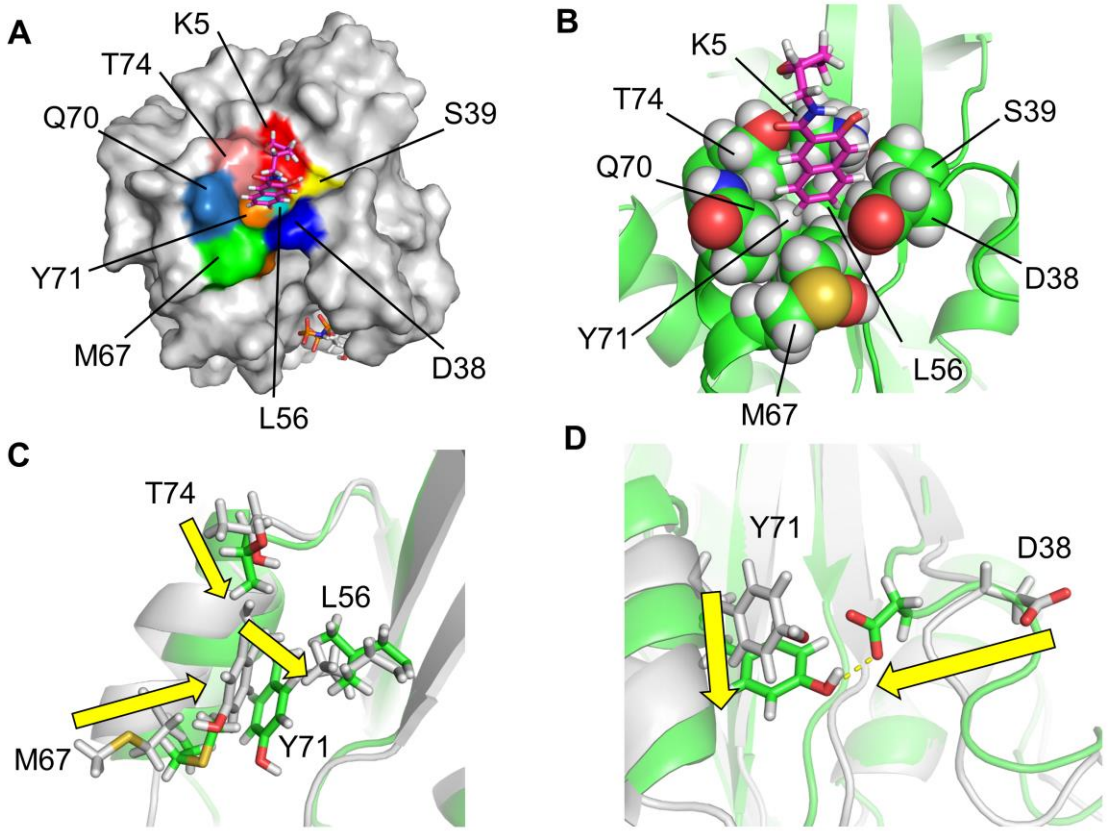

FIGURE 5. Formation of the KBFM123 binding site accompanied by the conformational changes. *A*, Molecular surface representation of H-RasT35S•GppNHp in complex with KBFM123. GppNHp and KBFM123 are shown in stick models. Also shown are Lys5 (*red*), Asp38 (*blue*), Ser39 (*yellow*), Leu56 (*cyan*), Met67 (*green*), Gln70 (*light blue*), Tyr71 (*orange*) and Thr74 (*pink*). *B*, Close-up view of the hydrophobic cluster. The side-chains of the residues forming the hydrophobic cluster are shown in the sphere models where nitrogen, oxygen and sulfur atoms are colored by blue, red and yellow, respectively. KBFM123 is shown in a stick model. Structural comparison of Leu56, Met67, Tyr71 and Thr74 (*C*) and Asp38 and Tyr71 (*D*) between H-RasT35•GppNHp in the the presence (*green*) or absence (*grey*) of KBFM123. The conformational changes induced by KBFM123-binding are indicated by yellow arrows. In (*D*), the representative structure forming interaction between Asp38 and Tyr71, which is indicated by yellow dashed line, is shown.

KBFM123-Induced Conformational Change in the Effector-Binding Region----The KBFM123-binding affected the structures of Switch I and its flanking region in the β2-strand (Fig. 4*B, C*), which are directly involved in recognition of the RBDs of the downstream effector molecules including c-Raf-1 (Fig. 6*A*) [2, 3, 10]. In particular, Asp38, which underwent a conformational change to form the KBFM123-binding site, made a salt bridge with Arg89, an essential residue for the interaction with c-Raf-1-RBD [3, 10, 18]. This suggested that the binding of KBFM123 to Ras•GTP would allosterically inhibit the c-Raf-1 interaction by impairing the formation of the scaffold necessary for the effector recognition. Accordingly, we performed ELISA to test inhibition of the binding of H-RasG12V•GppNHp to c-Raf-1 RBD and observed that KBFM123 indeed inhibited the binding in a dose-dependent manner with the estimated K_i value of 10^{-4}~10^{-5} M (Fig. 6*B*). Apparently blunted inhibition at 2.0 mM was likely to be accounted for by the insolubility of KBFM123. Since KBFM123 bound to H-RasT35S•GppNHp failed to exhibit a significant collision with c-Raf-1 RBD (Fig. 6*A*), an allosteric mechanism was suggested to be involved in the inhibition. Such an inhibitory mechanism is unprecedented and this makes the naphthalene a promising scaffold for generating novel Ras inhibitors.

Figure 6

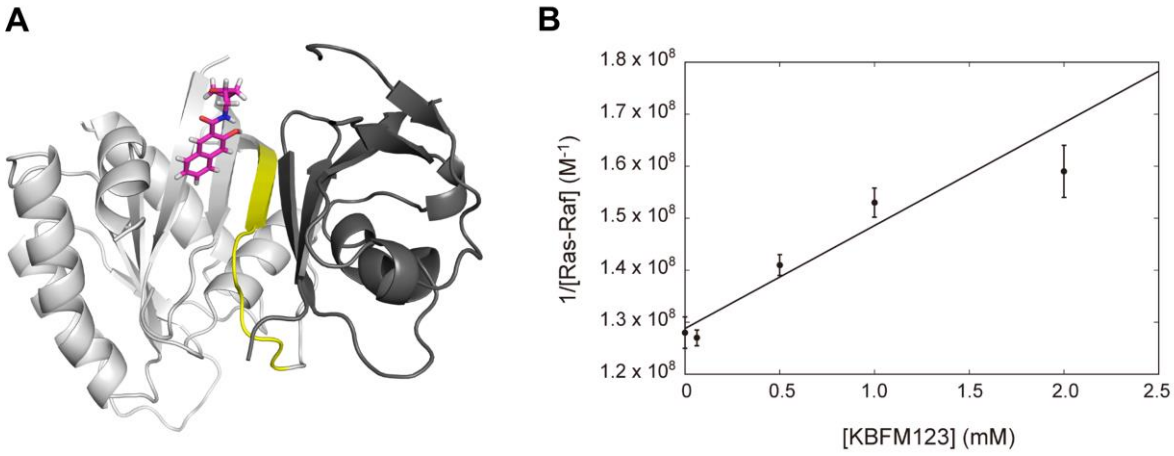

FIGURE 6. Inhibition of the c-Raf-1-RBD-binding by KBFM123. *A*, Superimposition of KBFM123 in the present structure with the complex of H-RasWT•GppNHp and c-Raf-1-RBD (PDB code 4G0N). H-RasWT•GppNHp, c-Raf-1-RBD and KBFM123 are colored in grey, dark grey and magenta, respectively. Switch I and the unstructured region of the β2-strand observed in this study are indicated by a yellow color. *B*, Kinetic analysis of the inhibition of Ras-Raf binding by KBFM123. Reciprocal values of the concentrations of full-length H-RasG12V•GppNHp bound to c-Raf-1-RBD (1/[Ras-Raf]), which were quantified from the dataset of the ELISA-based inhibitory assays, are plotted against the concentration of KBFM123 ([KBFM123]). The data fitting was carried out according to Ref. 16 and the apparent K_i value was estimated as 10^{-4}~10^{-5} M. The nonlinear increase in the reciprocal value at the

higher concentration of KBFM123 is possibly attributed to its low solubility. Error bars indicate the standard deviations from the mean (n = 4).

DISCUSSION

In the present study, we identified KBFM123 as a small-molecule compound interacting with H-Ras•GTP., NMR-based binding experiments and solution structure determination of its complex with H-RasT35S•GppNHp demonstrated that the naphthalene ring of KBFM123 interacts with a hydrophobic pocket lying between Switch I and Switch II, consisting of Lys5, Asp38, Ser39, Leu56, Met67, Gln70, Tyr71 and Thr74, which are completely conserved among H-Ras, K-Ras and N-Ras. This suggests that KBFM123 binds to all the Ras isoforms. Previous studies had shown that a wide variety of small-molecule compounds bound to the region nearly identical to that found in the present study, indicating the broad binding capacity of this hydrophobic pocket [20-22]. Among them, it is noteworthy that a thiol-reactive naphthalene, attached covalently to the Cys39 residue of a K-RasS39C mutant, was reported [21]. Although the thiol-reactive naphthalene ring of this compounds made hydrophobic interaction with Leu56, Met67, Tyr71 and Thr74 as observed with KBFM123, its orientation was distinct from that of KBFM123 (Fig. 7*A*). It is likely that the binding mode of this naphthalene ring is significantly restricted by the covalent bonding with Cys39 compared to that of KBFM123. In KBFM123, the two substituents in the naphthalene ring were oriented toward the bulk solvent (Fig. 5*A*, *B*), suggesting that they could become promising candidates for chemical modifications useful for fragment-based drug design.

Among the residues forming the KBFM123-binding region, Asp38, Met67, Tyr71 and Thr74 underwent conformational changes in response to the complex formation (Fig. 5*C, D*). Moreover, titration with KBFM123 induced a nonlinear change in the NH signal of Asp57, which was surrounded by Asp38, Leu56 and Tyr71 (Fig. 2). Considering from these structural changes, it is inferred that the nonlinear change represents a two-step binding reaction, *i. e.* formation of a transient complex by a low affinity interaction, which is followed by a conformational change to stabilize the complex. In this situation, the local magnetic environment around Asp57 would be strongly affected by the closely approaching naphthalene moiety of KBFM123 and subsequently by the side-chain of Tyr71 undergoing a conformational change. These structural alterations building the KBFM123-binding site would be propagated to make the N-terminal half of the β2-strand unstructured. Structural changes of this kind have not been observed for other small-molecule Ras inhibitors bound to the same hydrophobic pocket such as DCAI and the thiol-reactive naphthalene [20,22].

KBFM123 inhibited the binding of c-Raf-1-RBD to H-RasG12V•GppNHp although it was unlikely to make direct contact with c-Raf-1 RBD (Fig. 6*A, B*), suggesting that its inhibition mechanism is distinct from that of the previously reported Kobe-family compounds [16]. The inhibitory activity of KBFM123 was too weak to carry out kinetic interpretation of the binding data. Nevertheless, judging

from the solution structure of the complex with H-RasT35S•GppNHp, the inhibition was likely to be achieved by an allosteric mechanism via disruption of the c-Raf-1-RBD binding scaffold, including the conformational change of Asp38, on Ras•GTP, which was composed of Switch I and the neighboring regions. Because we used the state 1-predominating H-RasT35S•GppNHp for the structural characterization, it remains unclear whether KBFM123 binding induces similar inactivating structural changes into the state 2 conformation. However, it seems certain that KBFM123 is capable of associating with state 2 and inhibiting its interaction with c-Raf-1 RBD because it bound to the state 2-favoring H-RasWT•GppNHp as well (Fig. S1) and inhibited the c-Raf-1-RBD binding of H-RasG12V•GppNHp (Fig. 6*B*). This is also consistent with our observation that the estimated binding regions of KBFM123 were different from the regions whose structures were considerably affected by the state transition [9]. As anticipated from its low molecular weight, the inhibitory activity of KBFM123 was rather weak. In such case, application of fragment-based approaches would be promising to improve the potency of KBFM123. For this purpose, introduction of various substituents into the naphthalene ring at the position, which were oriented toward the bulk solvent and not much involved in the interaction with Ras•GTP, could be effectively utilized. The KBFM123-binding site is surrounded by the regions essential for the effector interaction such as the two Switch regions (Fig. 7*B*). The extension of the KBFM123 structure toward the Switch regions would result in direct interference with the effector binding and potentiation of KBFM123. In this regard, linking or merging of the naphthalene ring with the previously reported compounds, directly blocking the interaction with the upstream and downstream effectors, such as Kobe0065 and the indole-based compound 13 [16, 21], would be expected to improve their potencies (Fig. S7). To efficiently advance such compound development, dynamic nature of the complex should be taken into account since it is likely that the naphthalene ring is capable of adopting diverse orientations as found in a thiol-reactive naphthalene. The structural basis for the allosteric inhibition of Ras•GTP by a naphthalene-containing compound clarified by this study may provide a clue to generate novel Ras inhibitors with a potency suitable for clinical application.

Figure 7

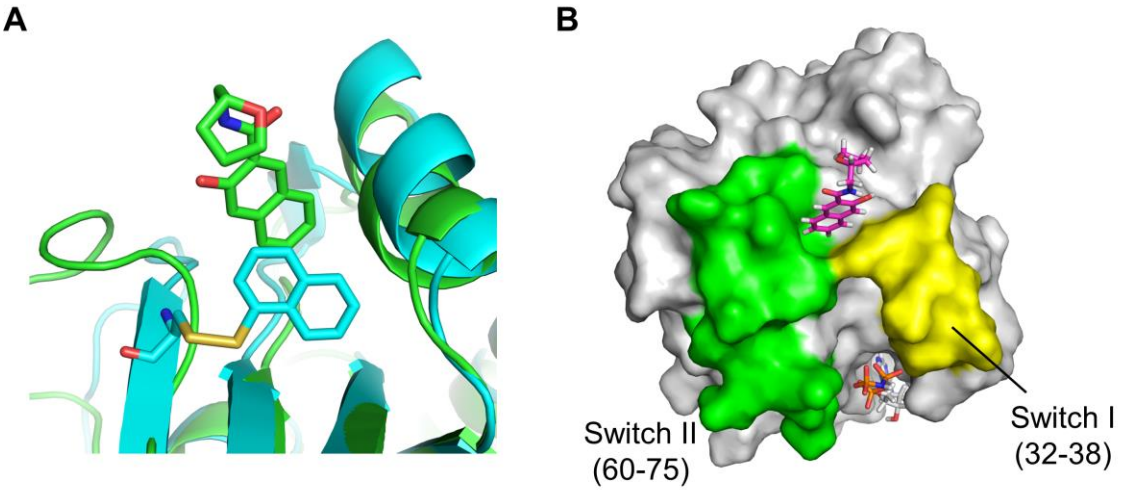

FIGURE 7. Potential of KBFM123 as a scaffold for the development of Ras inhibitors. *A,* Superimposition of the present structure (*green*) and the tertiary structure of K-RasS39C mutant covalently complexed with the thiol-reactive naphthalene (*cyan*, PDB code 4Q01). KBFM123, the thiol-reactive naphthalene and Cys39 in K-RasS39C mutant are represented by stick models. *B,* The molecular surface representation of H-RasT35S•GppNHp in complex with KBFM123. Switch I and Switch II are indicated by yellow and green colors, respectively. KBFM123 and GppNHp are represented by stick models.

Acknowledgements: We thank Kenjiro Matsuo, Syuichi Tsukamoto and Syuichiro Tanabe for technical assistance.

SUPPORTING INFORMATION:

Figure S1. The ^{1}H-^{15}N HSQC spectra of the representative residues exhibiting NH signal changes induced by the KBFM123-binding in H-RasT35S•GppNHp and H-RasWT•GppNHp.

Figure S2. Superimposition of the tertiary structures of H-Ras•GppNHp in state 1 and state 2.

Figure S3. Assignments of the proton signals in KBFM123.

Figure S4. The CSPs of the NH signals induced by the binding of the naphthalene analogs, KBFM59 and KBFM198.

Figure S5. The ^{1}H-^{15}N HSQC spectra of the representative residues exhibiting NH signal changes induced by the binding of KBFM123, KBFM59 and KBFM198 to H-RasT35S•GppNHp.

Figure S6. Comparison of the side chains of Asp38, Leu56, Met67, Tyr71 and Thr74 in ensemble structures between H-RasT35•GppNHp in the presence or absence of KBFM123.

Figure S7. Relative positions among KBFM123, Kobe0065 and the indole-based compound 13 complexed with H-Ras.

Table S1. Lists of intermolecular NOEs between the protons of the naphthalene ring and those of H-RasT35S•GppNHp.

Conflict of interest: The authors declare that they have no conflict of interest with the contents of this article.

Author contributions: SM, FS, MN, MA and TK designed the study and analyzed the data. SM, TH and YH conducted most of the experiments. YY and CT conducted a part of the experiments. TK conceived the idea for the project and wrote the paper with SM. All the authors reviewed the results and approved the final version of the manuscript.

REFERENCES

1. Karnoub, A. E., and Weinberg, R. A. (2008) Ras oncogenes: split personalities. *Nat. Rev. Mol. Cell. Biol.* **9**, 517-531

2. Huang, L., Hofer, F., Martin, G. S., and Kim, S. H. (1998) Structural basis for the interaction of Ras with RalGDS. Nat. Struct. Biol. **5**, 422-426

3. Nassar, N., Horn, G., Herrmann, C., Scherer, A., McCormick, F., and Wittinghofer, A. (1995) The 2.2 Å crystal structure of the Ras-binding domain of the serine/threonine kinase c-Raf1 in complex with Rap1A and a GTP analogue. *Nature* **375**, 554-560

4. Pacold, M. E., Suire, S., Perisic, O., Lara-Gonzalez, S., Davis, C. T., Walker, E. H., Hawkins, P. T., Stephens, L., Eccleston, J. F., and Williams, R. L. (2000) Crystal structure and functional analysis of Ras binding to its effector phosphoinositide 3-kinase γ. *Cell* **103**, 931-943

5. Vetter, I. R., and Wittinghofer, A. (2001) The guanine nucleotide-binding switch in three dimensions. *Science* **294**, 1299-1304

6. Geyer, M., Schweins, T., Herrmann, C., Prisner, T., Wittinghofer, A., and Kalbitzer, H. R. (1996) Conformational transitions in p21ras and in its complexes with the effector protein Raf-RBD and the GTPase activating protein GAP. *Biochemistry* **35**, 10308-10320

7. Spoerner, M., Hozsa, C., Poetzl, J. A., Reiss, K., Ganser, P., Geyer, M., and Kalbitzer, H. R. (2010) Conformational states of human rat sarcoma (Ras) protein complexed with its natural ligand GTP and their role for effector interaction and GTP hydrolysis. *J. Biol. Chem.* **285**, 39768-39778

8. Spoerner, M., Herrmann, C., Vetter, I. R., Kalbitzer, H. R., and Wittinghofer, A. (2001) Dynamic properties of the Ras switch I region and its importance for binding to effectors. *Proc. Natl. Acad. Sci. U.S.A.* **98**, 4944-4949

9. Matsumoto, S., Miyano, N., Baba, S., Liao, J., Kawamura, T., Tsuda, C., Takeda, A., Yamamoto, M., Kumasaka, T., Kataoka, T., and Shima, F. (2016) Molecular mechanism for conformational dynamics of Ras•GTP elucidated from in-situ structural transition in crystal. *Sci. Rep.* **6**, 25931.

10. Fetics, S. K., Guterres, H., Kearney, B. M., Buhrman, G., Ma, B., Nussinov, R., and Mattos, C. (2015) Allosteric effects of the oncogenic RasQ61L mutant on Raf-RBD. *Structure* **23**, 505-516

11. Pai, E. F., Kabsch, W., Krengel, U., Holmes, K. C., John, J., and Wittinghofer, A. (1989) Structure of the guanine-nucleotide-binding domain of the Ha-ras oncogene product p21 in the triphosphate conformation. *Nature* **341**, 209-214

12. Pai, E. F., Krengel, U., Petsko, G. A., Goody, R. S., Kabsch, W., and Wittinghofer, A. (1990) Refined crystal structure of the triphosphate conformation of H-ras p21 at 1.35 Å resolution: implications for the mechanism of GTP hydrolysis. *EMBO J.* **9**, 2351-2359

13. Spoerner, M., Nuehs, A., Herrmann, C., Steiner, G., and Kalbitzer, H. R. (2007) Slow conformational dynamics of the guanine nucleotide-binding protein Ras complexed with the GTP analogue GTPγS. *FEBS J.* **274**, 1419-1433

14. Araki, M., Shima, F., Yoshikawa, Y., Muraoka, S., Ijiri, Y., Nagahara, Y., Shirono, T., Kataoka, T., and Tamura, A. (2011) Solution structure of the state 1 conformer of GTP-bound H-Ras protein and

distinct dynamic properties between the state 1 and state 2 conformers. *J. Biol. Chem.* **286**, 39644-39653

15. Shima, F., Ijiri, Y., Muraoka, S., Liao, J., Ye, M., Araki, M., Matsumoto, K., Yamamoto, N., Sugimoto, T., Yoshikawa, Y., Kumasaka, T., Yamamoto, M., Tamura, A., and Kataoka, T. (2010) Structural basis for conformational dynamics of GTP-bound Ras protein. *J. Biol. Chem.* **285**, 22696-22705

16. Shima, F., Yoshikawa, Y., Ye, M., Araki, M., Matsumoto, S., Liao, J., Hu, L., Sugimoto, T., Ijiri, Y., Takeda, A., Nishiyama, Y., Sato, C., Muraoka, S., Tamura, A., Osoda, T., Tsuda, K., Miyakawa, T., Fukunishi, H., Shimada, J., Kumasaka, T., Yamamoto, M., and Kataoka, T. (2013) *In silico* discovery of small-molecule Ras inhibitors that display antitumor activity by blocking the Ras-effector interaction. *Proc. Natl. Acad. Sci. U.S.A.* **110**, 8182-8187

17. Kabsch, W., and Sander, C. (1983) Dictionary of protein secondary structure: pattern recognition of hydrogen-bonded and geometrical features. *Biopolymers* **22**, 2577-2637

18. Hyberts, S. G., Goldberg, M. S., Havel, T. F., and Wagner, G. (1992) The solution structure of eglin c based on measurements of many NOEs and coupling constants and its comparison with X-ray structures. *Prot. Sci.* **1**, 736-751

19. Block, C., Janknecht, R., Herrmann, C., Nassar, N., and Wittinghofer, A. (1996) Quantitative structure-activity analysis correlating Ras/Raf interaction in vitro to Raf activation *in vivo*. *Nat. Struct. Biol.* **3**, 244-251

20. Maurer, T., Garrenton, L. S., Oh, A., Pitts, K., Anderson, D. J., Skelton, N. J., Fauber, B. P., Pan, B., Malek, S., Stokoe, D., Ludlam, M. J., Bowman, K. K., Wu, J., Giannetti, A. M., Starovasnik, M. A., Mellman, I., Jackson, P. K., Rudolph, J., Wang, W., and Fang, G. (2012) Small-molecule ligands bind to a distinct pocket in Ras and inhibit SOS-mediated nucleotide exchange activity. *Proc. Natl. Acad. Sci. U.S.A.* **109**, 5299-5304

21. Sun, Q., Burke, J. P., Phan, J., Burns, M. C., Olejniczak, E. T., Waterson, A. G., Lee, T., Rossanese, O. W., and Fesik, S. W. (2012) Discovery of small molecules that bind to K-Ras and inhibit Sos-mediated activation. *Angew. Chem. Int. Ed. Engl.* **51**, 6140-6143

22. Sun, Q., Phan, J., Friberg, A. R., Camper, D. V., Olejniczak, E. T., and Fesik, S. W. (2014) A method for the second-site screening of K-Ras in the presence of a covalently attached first-site ligand. *J. Biomol. NMR* **60**, 11-14

23. Liao, J., Shima, F., Araki, M., Ye, M., Muraoka, S., Sugimoto, T., Kawamura, M., Yamamoto, N., Tamura, A., and Kataoka, T. (2008) Two conformational states of Ras GTPase exhibit differential GTP-binding kinetics. *Biochem. Biophys. Res. Commun.* **369**, 327–332

24. Delaglio, F., Grzesiek, S., Vuister, G. W., Zhu, G., Pfeifer, J., and Bax, A. (1995) NMRPipe: a multidimensional spectral processing system based on UNIX pipes. *J. Biomol. NMR* **6**, 277-293

25. Brunger, A. T., Adams, P. D., Clore, G. M., DeLano, W. L., Gros, P., Grosse-Kunstleve, R. W., Jiang, J. S., Kuszewski, J., Nilges, M., Pannu, N. S., Read, R. J., Rice, L. M., Simonson, T., and Warren, G. L. (1998) Crystallography & NMR system: A new software suite for macromolecular

structure determination. *Acta Crystallogr. D Biol. Crystallogr.* **54**, 905-921

26. Kleywegt, G. J. (2007) Crystallographic refinement of ligand complexes. *Acta Crystallogr. D Biol. Crystallogr.* **63**, 94-100

27. Laskowski, R. A., Rullmannn, J. A., MacArthur, M. W., Kaptein, R., and Thornton, J. M. (1996) AQUA and PROCHECK-NMR: programs for checking the quality of protein structures solved by NMR. *J. Biomol. NMR* **8**, 477-486

28. Koradi, R., Billeter, M., and Wuthrich, K. (1996) MOLMOL: a program for display and analysis of macromolecular structures. *J. Mol. Graph.* **14**, 51-55

FOOTNOTES

This work was supported by grants from the Ministry of Health, Labor and Welfare and Japan Agency for Medical Research and Development (AMED) (grant number 15ak0101006h0005) and from the National Institute of Biomedical Innovation (NIBIO) and AMED (grant number 15nk0101401h0002).

[1]The abbreviations used are: PI3K, phosphatidylinositol 3-kinase; RalGDS, Ral guanine nucleotide-dissociation stimulator; GEF, guanine nucleotide exchange factor; GAP, GTPase-activating protein; GppNHp, guanosine 5'-(β, γ-imido)triphosphate; RBD, Ras-binding domain; WT, wild type; GST, glutathione-*S*-transferase; DMSO, dimethyl sulfoxide; COSY, correlation spectroscopy; HSQC, hetero-nuclear single quantum coherence; HMBC, hetero-nuclear multiple quantum coherence; NOE, nuclear overhauser effect; NOESY, NOE spectroscopy; CSP, chemical shift perturbation; STD, saturation transfer difference; ELISA, enzyme-linked immunosorbent assay.

TABLE 1. Structural statistics for the 15 lowest energy structures of the H-RasT35S•GppNHp-KBFM123 complex.

Number of distance restraints	
Total	2591
Intramolecular NOEs (H-RasT35S•GppNHp)	
Intraresidue	706
Short-range (|*i-j*| = 1 residues)	644
Medium-range (|*i-j*| = 2 to 4 residues)	426
Long-range (|*i-j*| > 4 residues)	800
Intermolecular NOEs	15
Number of torsion angle restraints	
ϕ / ψ	124 / 124
RMSD from ideal covalent geometry	
Bond lengths (Å)	0.0014 ± 0.000074
Bond angles (°)	0.31 ± 0.0065
Impropers (°)	0.24 ± 0.0067
RMSD from the mean structure (Å)	
Backbone atoms (residues 1-9, 15-30, 39-59, 76-105, 108-119, 123-166)	0.47 ± 0.08
All heavy atoms (residues 1-9, 15-30, 39-59, 76-105, 108-119, 123-166)	1.20 ± 0.16
Backbone atoms (residues 1-166)	0.72 ± 0.11
All heavy atoms (residues 1-166)	1.45 ± 0.18
Ramachandran analysis	
Most favored regions (%)	90.2
Additional allowed regions (%)	9.0
Generously allowed regions (%)	0.0
Disallowed regions (%)	0.8

Ramachandran analysis for the regions, 1-9, 15-30, 39-59, 76-105, 108-119 and 123-166, was carried out by the program PROCHECK [27].

Molecular Basis for Allosteric Inhibition of GTP-Bound H-Ras Protein by a Small-Molecule Compound Carrying a Naphthalene Ring

Shigeyuki Matsumoto[1, 3], Toshiki Hiraga[1], Yuki Hayashi[1], Yoko Yoshikawa[1], Chiemi Tsuda[1], Mitsugu Araki[2, 4], Masahiro Neya[2], Fumi Shima[1, 5], and Tohru Kataoka[1, 6]

[1]Division of Molecular Biology, Department of Biochemistry and Molecular Biology, Kobe University Graduate School of Medicine

[2]Medicinal Frontier Dept., KNC Laboratories Co., Ltd.

[3]Present address: RIKEN Cluster for Science, Technology and Innovation Hub

[4]Present address: Graduate School of Medicine, Kyoto University

[5]Present address: Drug Discovery Science, Division of Advanced Medical Science, Department of Science, Technology and Innovation, Graduate School of Science, Technology and Innovation, Kobe University

[6]Present address: Kobe University Incubation Center

SUPPORTING INFORMATION

Figure S1

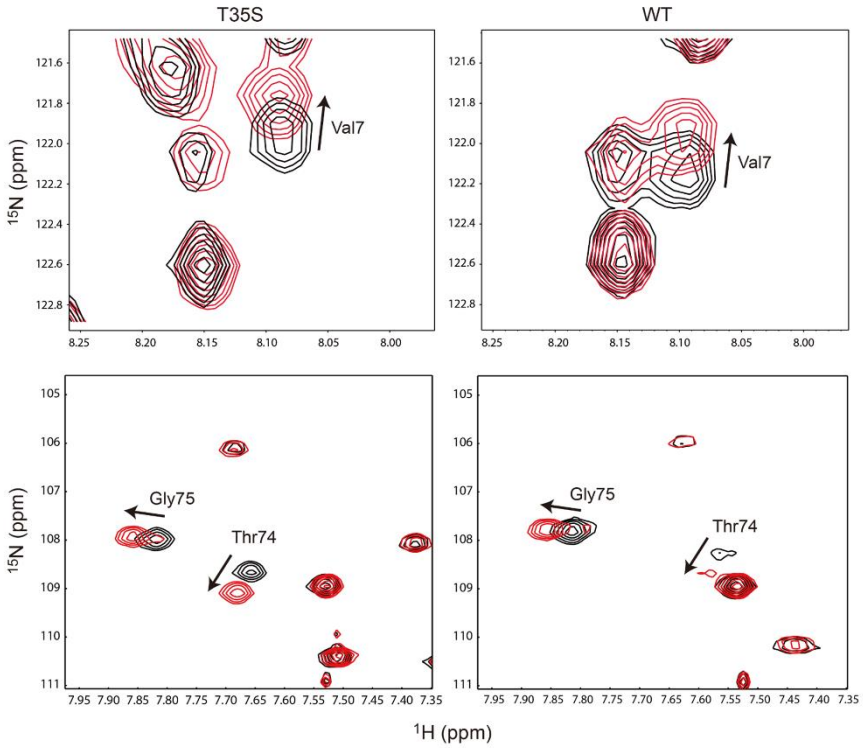

Fig. S1. The ^{1}H-^{15}N HSQC spectra of the representative residues exhibiting NH signal changes induced by the KBFM123-binding in H-RasT35S•GppNHp and H-RasWT•GppNHp. The ^{1}H-^{15}N HSQC spectra in the absence of and in the presence of KBFM123 are colored in black and red, respectively. The NH signal of Thr74 in H-RasWT•GppNHp is significantly broadened due to the conformational exchange on a millisecond time scale.

Figure S2

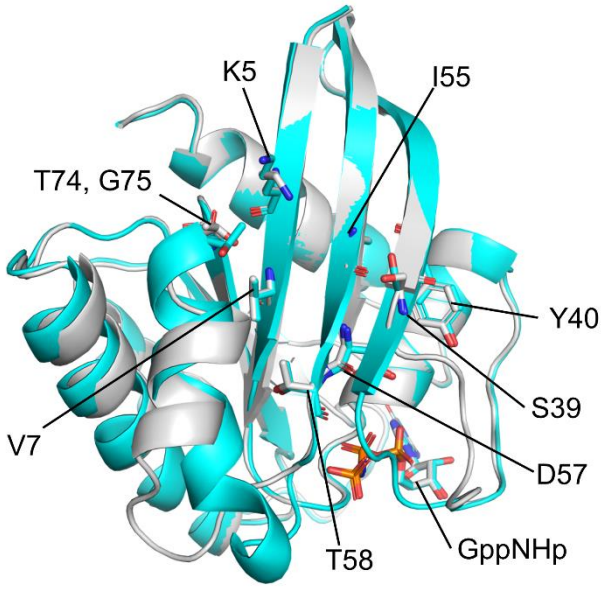

Fig. S2. Superimposition of the tertiary structures of H-Ras•GppNHp in state 1 (PDB code 5B30, *grey*) and state 2 (PDB code 3K8Y, *cyan*). The residues showing significant CSPs in the estimated binding region of KBFM123: Lys5, Val7, Ser39, Tyr40, Ile55, Asp57, Thr58, Thr74 and Gly75, and GppNHp are shown in stick models where nitrogen and oxygen atoms are colored by blue and red, respectively.

Figure S3

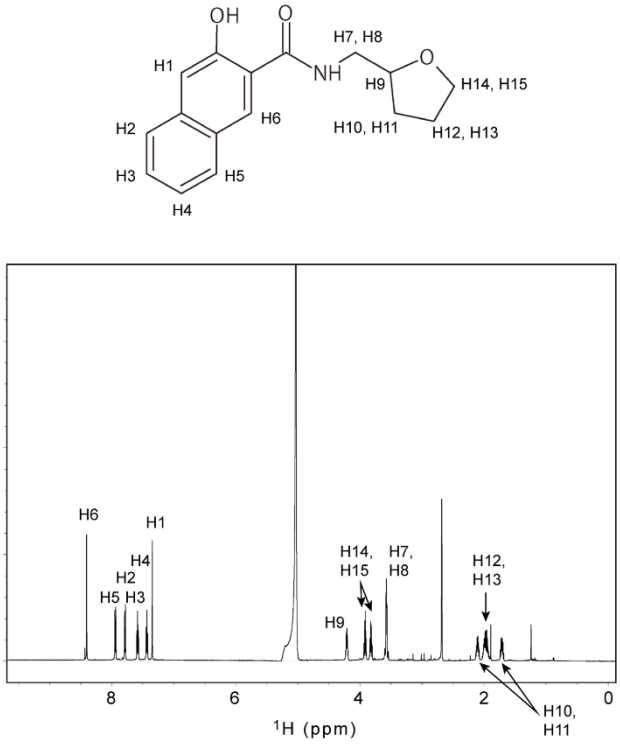

Fig. S3. Assignments of the proton signals in KBFM123.

Figure S4

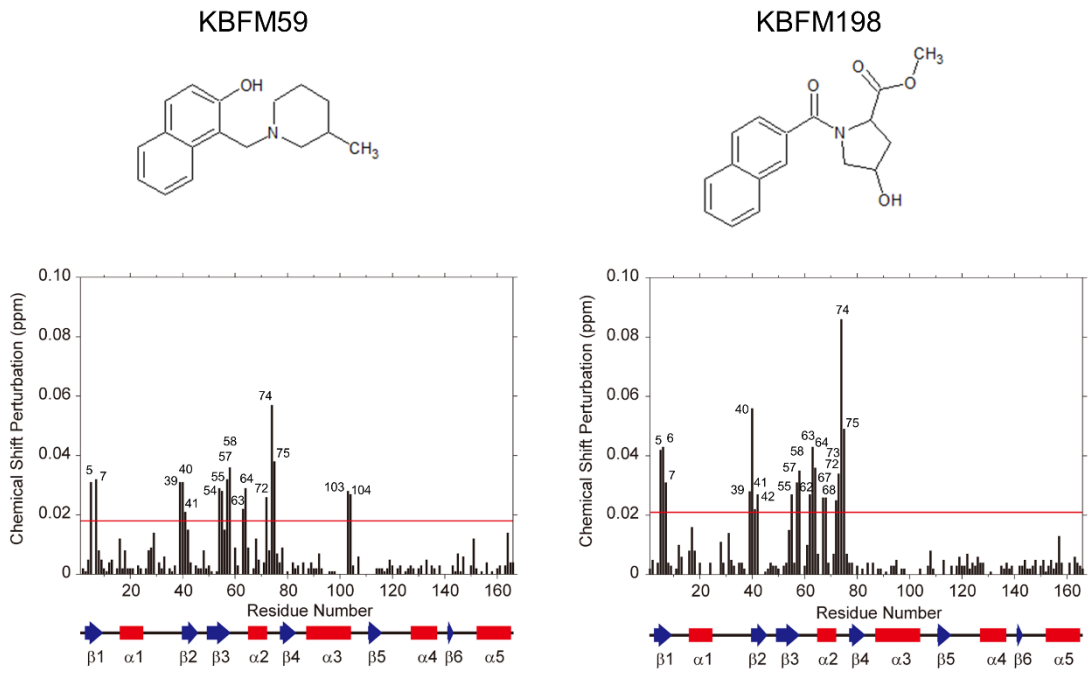

Fig. S4. The CSPs of the NH signals induced by the binding of the naphthalene analogs, KBFM59 and KBFM198. The red horizontal line indicates the sum of the average and the standard deviation. A diagram representing the secondary structure of H-RasT35S•GppNHp (PDB code 2LCF) is shown at the bottom, where α-helices and β-strands are indicated by red rectangles and blue arrows, respectively. The apparent concentration of the compounds is 4 mM.

Figure S5

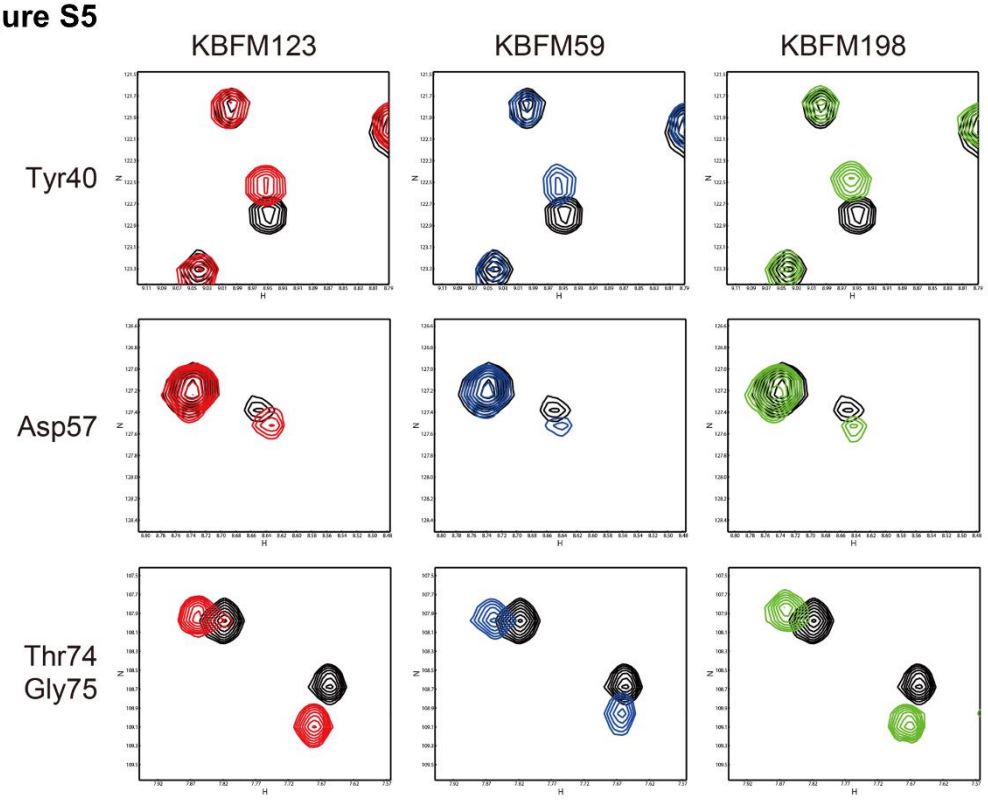

Fig. S5. The ^{1}H-^{15}N HSQC spectra of the representative residues exhibiting NH signal changes induced by the binding of KBFM123 (*red)*, KBFM59 (*blue*) and KBFM198 (*green*) to H-RasT35S•GppNHp. The spectra in the presence of the naphthalene analogs are overlaid with that of H-RasT35S•GppNHp in the absence of the compounds (*black*).

Figure S6

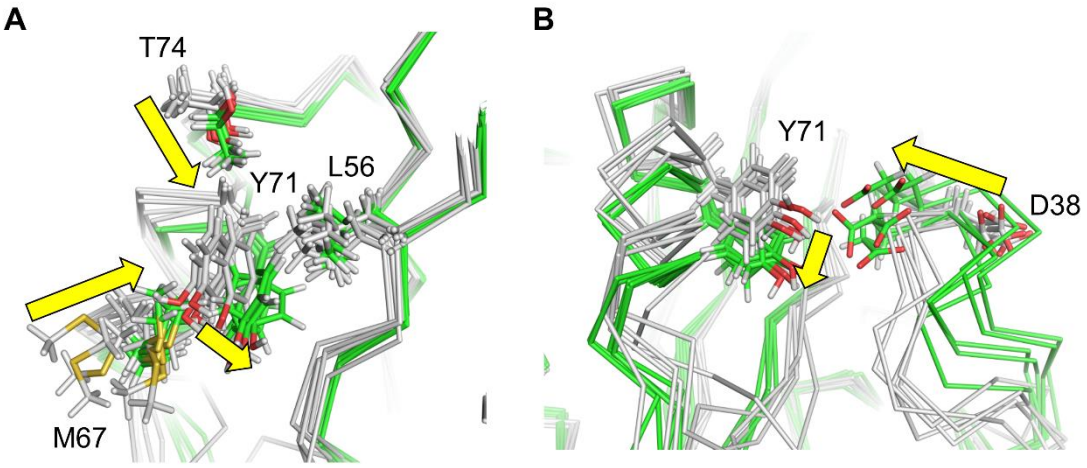

Fig. S6. Comparison of the side chains of Leu56, Met67, Tyr71 and Thr74 (A) and Asp38 and Tyr71 (B) in ensemble structures between H-RasT35•GppNHp in the presence (*green*) or absence (*grey*) of KBFM123. The representative 5 structures in the ensemble structures are superimposed and the side chains of Asp38 and Tyr71 and the trace of their main-chains are represented by stick models.

Figure S7

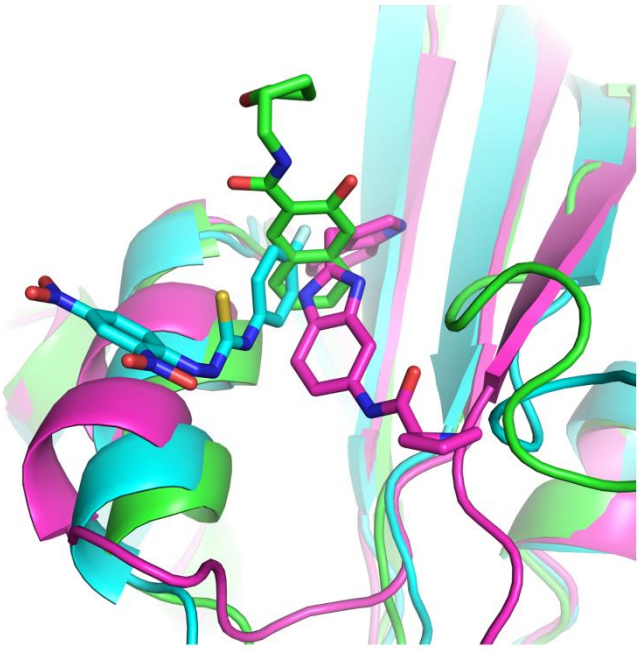

Fig. S7. Relative positions among KBFM123 (*green*), Kobe0065 (*cyan*) and the indole-based compound 13 (*magenta*) complexed with H-Ras. The compounds are indicated by stick models where nitrogen, oxygen and sulfur atoms are colored by blue, red and yellow, respectively.

TABLE S1. Intermolecular NOEs between the protons of the naphthalene ring and those of H-RasT35S•GppNHp

Protons in H-RasT35S・GppNHp	Protons in KBFM123[a]
Lys5 ε	H3
Lys5 ε	H4
Lys5 ε	H5
Lys5 ε	H6
Val7 γ2	H3
Val7 γ2	H4
Leu56 δ2	H3
Leu56 δ2	H4
Met67 ε	H3
Met67 ε	H4
Met67 ε	H5
Thr74 γ2	H3
Thr74 γ2	H4
Thr74 γ2	H5
Thr74 γ2	H6

[a]The names of the protons in KBFM123 are shown in Fig. S3.